JACS
JOURNAL OF THE AMERICAN CHEMICAL SOCIETY
Article
pubs.acs.org/JACS

Transition-State Enthalpy and Entropy Effects on Reactivity and Selectivity in Hydrogenolysis of *n*-Alkanes

David W. Flaherty and Enrique Iglesia*

Department of Chemical Engineering, University of California at Berkeley, Berkeley, California 94720, United States

Supporting Information

ABSTRACT: Statistical mechanics and transition state (TS) theory describe rates and selectivities of C−C bond cleavage in C_2−C_{10} *n*-alkanes on metal catalysts and provide a general description for the hydrogenolysis of hydrocarbons. Mechanistic interpretation shows the dominant role of entropy, over enthalpy, in determining the location and rate of C−C bond cleavage. Ir, Rh, and Pt clusters cleave C−C bonds at rates proportional to coverages of intermediates derived by removing 3−4 H-atoms from *n*-alkanes. Rate constants for C−C cleavage reflect large activation enthalpies ($\Delta H^{\ddagger}$, 217−257 kJ mol^{-1}) that are independent of chain length and C−C bond location in C_{4+} *n*-alkanes. C−C bonds cleave because of large, positive activation entropies ($\Delta S^{\ddagger}$, 164−259 J mol^{-1} K^{-1}) provided by H_2 that forms with TS. Kinetic and independent spectroscopic evidence for the composition and structure of these TS give accurate estimates of $\Delta S^{\ddagger}$ for cleavage at each C−C bond. Large differences between rate constants for ethane and n-decane (~10^8) reflect an increase in the entropy of gaseous alkanes retained at the TS. The location of C−C bond cleavage depends solely on the rotational entropies of alkyl chains attached to the cleaved C−C bond, which depend on their chain length. Such entropy considerations account for the ubiquitous, but previously unexplained, preference for cleaving nonterminal C−C bonds in *n*-alkanes. This mechanistic analysis and thermodynamic treatment illustrates the continued utility of such approaches even for hydrogenolysis reactions, with complexity seemingly beyond the reach of classical treatments, and applies to catalytic clusters beyond those reported here (0.6−2.7 nm; Ir, Rh, Pt).

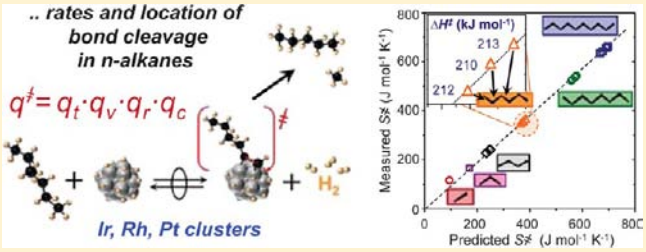

1. INTRODUCTION

The catalytic hydrogenolysis of alkanes, especially ethane, butane, and substituted cyclopentanes, has been extensively studied[1−9] since the initial reports of ethane hydrogenolysis on surfaces of Fe and Ni clusters by Taylor et al.[10−12] and the seminal findings on ring-opening reactions of substituted cyclopentanes on Pt[8,13] and Ir[14] clusters by Gault et al.[15] Hydrogenolysis of alkanes is considered a prototypical structure-sensitive reaction, for which turnover rates, activation energies, and the identity of adsorbed and reactive species depend strongly on the identity[16−20] and the coordinative saturation of the atoms exposed at metal cluster surfaces.[2,8,15,21−27] The location of C−C bond cleavage in alkanes depends on temperature (because of differences in activation enthalpies), on H_2 and alkane pressures, on the identity of the catalytic metal, on the coordinative unsaturation of exposed metals atoms, which varies with cluster size, and on the substitution of the C-atoms at a given C−C bond.[15,28−34] These effects determine the selectivity in reactions that cleave C−C, C−S, and C−O bonds present in reactants derived from fossil or biomass resources, for which catalytic processes improve their energy density and fuel quality, while removing heteroatom contaminants.[3,34−38]

Broad concepts and unifying principles that describe reactivity and selectivity in catalytic hydrogenolysis have remained elusive; in particular, as they seek connections between simpler molecules, such as ethane, and molecules more relevant to industrial practice, such as larger *n*-alkanes, isoalkanes, and cycloalkanes. The large body of previous work does not provide clear guidance about how kinetic effects of temperature, reactant coverage, alkane and cycloalkane structure, and metal cluster size or identity lead, in turn, to hydrogenolysis turnover rates and C−C bond cleavage selectivities. Here, we seek such guidance for hydrogenolysis of *n*-alkanes on Ir, Rh, and Pt clusters through rigorous mechanistic interpretations of turnover rates and selectivities using the formalism of transition state theory.

The sequence of elementary steps proposed here describes *n*-alkane (C_2−C_{10}) hydrogenolysis rates, while providing evidence for the extent of dehydrogenation of the intermediates involved in the cleavage of specific C−C bonds. The resulting rate equation contains equilibrium and rate constants for elementary steps, which reflect the chemical origins of the observed reactivity and concomitant differences between the Gibbs free energy of the reactant alkane and adsorbed H-atoms (H*) and that of the product H_2, formed by desorbing 2H* and dehydrogenating the alkane, and the kinetically relevant transition state. Activation enthalpies ($\Delta H^{\ddagger}$) reflect homolytic dissociation energies of C−C bonds in alkanes, and activation

Received: September 10, 2013
Published: November 22, 2013

   dx.doi.org/10.1021/ja4093743 | J. Am. Chem. Soc. 2013, 135, 18586−18599

Table 1. Synthesis Conditions and Characterization Results for Ir, Rh, and Pt Catalysts

			temp (K)		dispersion (%)				
sample	TEA:M[a]	metal content (% wt)	oxidative treatment[b]	reductive treatment[c]	H_2[d]	O_2[e]	CO[f]	$<d_{chem}>$[g] (nm)	$<d_{TEM}>$[h] (nm)
0.7 nm Ir	20	1.0	573, 1 h	873, 3 h	140	165	154	0.7	0.8
1.3 nm Ir	10	0.5	573, 1 h	973, 6 h	76	77		1.3	1.2
2.7 nm Ir	10	2.0	673, 2 h	723, 3 h	36	35		2.7	6.2
0.9 nm Rh	10	0.5	573, 1 h	723, 3 h	111	117	99	0.9	0.9
0.6 nm Pt	*i*	1.0		723, 3 h	155	160	151	0.6	0.7

[a]Molar ratio of triethanol amine to metal precursor in aqueous solution used for SiO_2 impregnation. [b]21 kPa O_2 (dry air). [c]50 kPa H_2 (balance He). [d]H_2 chemisorption (irreversible at 300 K), assuming H:M_s = 1. [e]O_2 chemisorption (irreversible at 300 K), assuming O:M_s = 1. [f]CO chemisorption (irreversible at 300 K), assuming CO:M_s = 1. [g]Mean particle diameters, d_{chem}, calculated from $d_{chem} = C/D$, where C is 0.99 for spherical clusters and D is the measured dispersion from irreversible H_2 uptakes [h]Surface-averaged mean cluster diameter from TEM analysis using $<d_{TEM}> = \sum n_i d_i^3 / \sum n_i d_i^2$. [i]Pt−$SiO_2$ was prepared using strong electrostatic adsorption and did not involve TEA.

entropies ($\Delta S^{\ddagger}$) depend, in part, on the entropy of transition states that we predict using the principles of statistical mechanics to describe a plausible transition-state structure. These data and their mechanistic interpretation provide evidence for the preeminent role of entropy in hydrogenolysis catalysis, which allows reactions with large activation barriers to proceed at modest temperatures. Identical series of elementary steps lead to C−C bond rupture at every position in each *n*-alkane, however, the statistical mechanics model predicts how small changes in transition state structures lead to consequential entropy differences that ultimately determine the location of C−C bond cleavage along the *n*-alkane backbone. We show here that these concepts are general to hydrogenolysis rates and selectivities of *n*-alkanes on surfaces of metal clusters and also describe the hydrogenolysis of isoalkanes and cycloalkanes, as we discuss in later reports.

2. METHODS AND CHARACTERIZATION RESULTS

2.1. Synthesis of Supported Ir, Rh, and Pt Catalysts. Silica [Davisil 646, 300 m^2 g^{-1}] was treated in flowing dry air (Praxair, 99.99%, 5.0 cm^3 g^{-1} s^{-1}) by heating to 823 at 0.03 K s^{-1} and holding for 5 h. Highly dispersed Ir complexes were deposited onto treated silica using incipient wetness impregnation with an aqueous solution of Ir complexes prepared by combining triethanolamine (TEA, Sigma-Aldrich, 97%) with H_2IrCl_6 (Strem Chemicals, 99%) (20:1 mol) in deionized (DI) water (17.9 MΩ resistivity), as reported previously for Ru catalysts.[39] Ir-SiO_2 (1.0% wt) was prepared by adding H_2IrCl_6 (0.424 g) to deionized water (21.2 cm^3) and then adding TEA (3.11 g). The resulting purple H_2IrCl_6 suspension turned clear olive-green upon TEA addition, consistent with replacement of Cl by TEA ligands. This clear solution (24.7 g) was added dropwise to the treated SiO_2 (20.0 g of Davisil 646). Ir−SiO_2 samples with different Ir loadings were prepared by changing the concentration of TEA and H_2IrCl_6 while maintaining a 20:1 mol ratio between these components. Rh−SiO_2 (0.5% wt) was prepared by impregnating SiO_2 (12.0 g of Davisil 646) with a solution containing TEA (0.72 g) and $Rh(NO_3)_3$ (0.140 g, Sigma-Aldrich, 99%) (10:1 mol) in DI water. Pt−SiO_2 (1.0% wt) was synthesized by strong-electrostatic adsorption of $Pt(NH_3)_4(NO_3)_2$ (0.400 g, Sigma-Aldrich, 99.9%) onto SiO_2 (20.0 g Davisil 646) from a 0.4 M NH_4OH solution (200 mL).[40] The solution was stirred for 2 h to allow cationic Pt complexes to adsorb. The solids were filtered and rinsed three times with 100 mL of DI water. All metal-loaded silica samples were heated to 393 at 0.017 K s^{-1} in flowing dry air and held for 8 h. The resulting dry Ir−SiO_2 and Rh−SiO_2 powders were heated to 573 at 0.017 K s^{-1} in flowing dry air and held for 1 h with the intent to condense TEA complexes with silanol groups on silica surfaces.[39] These samples were then heated to 673 at 0.033 K s^{-1} in flowing 50% H_2/He (Praxair, 99.999%, 1.0 cm^3 g^{-1} s^{-1}) and held for 3 h to decompose the precursors and form Ir and Rh metal clusters. The dry Pt−SiO_2 was heated to 723 at 0.017 K s^{-1} in flowing 50% H_2/He and held for 3 h to form Pt clusters. Samples were cooled to ambient temperature and passivated in flowing 0.5% O_2/He (Praxair, 99.99%, 1.0 cm^3 g^{-1} s^{-1}) for 6 h before exposure to ambient air. The dispersions of the Ir-SiO_2 were subsequently adjusted by oxidative and reductive treatments followed by passivation, as summarized in Table 1.

2.2. Metal Cluster Dispersion and Elemental Analysis. The mean diameters of supported Ir, Rh, and Pt clusters were determined using volumetric uptakes of H_2, O_2, and CO and transmission electron microscopy (TEM). Volumetric uptakes were measured at 298 K using a manual glass chemisorption unit. The sample was first treated in flowing H_2 (Praxair, 99.999%, 0.33 cm^3 g^{-1} s^{-1}) by heating to 598 at 0.083 K s^{-1} and holding for 1 h, after which, the sample was evacuated for 1 h at 598 K and cooled to 298 K. Uptakes were measured between 0.1 and 1 kPa H_2, and the sample was evacuated again at 298 K for 0.25 h. Uptakes were then measured again at the same conditions, and the difference between the two isotherms (after extrapolation to zero pressure) was defined as the irreversible hydrogen uptake. The irreversible adsorption of O_2 (Praxair, 99.99%) and CO (Praxair, 99.5%) were measured at 298 K as a single isotherm, following identical H_2 treatment and evacuation routines, and extrapolated to zero pressure to determine the total O_2 and CO uptakes. The number of exposed metal atoms (M_s) was estimated assuming adsorption stoichiometries of 1/1 for H/M_s, O/M_s, and CO/M_s.[41] The mean cluster diameter ($<d_{chem}>$) for each sample was estimated from the measured dispersion by assuming hemispherical crystallites and the atomic density of the bulk metals.[42,43] Dispersion values determined from H_2, O_2, and CO chemisorption are shown in Table 1. The metal content of each sample was measured by inductively coupled plasma optical emission spectroscopy (Galbraith Laboratories, Inc.).

The cluster size distribution was determined by TEM imaging in bright-field mode (Philips, CM200F) using samples applied as a fine dust onto Cu grids coated by "lacey" carbon. Surface-averaged cluster diameters were calculated using

$$<d_{TEM}> = \frac{\sum n_i d_i^3}{\sum n_i d_i^2} \quad (1)$$

where n_i is the number of clusters with a diameter d_i.[44] A representative TEM image and the cluster size distribution for the 0.7 nm Ir catalyst is shown in Figure 1, while TEM images and cluster size distributions for the other catalysts (1.3 nm Ir, 2.7 nm Ir, 0.9 nm Rh, and 0.6 nm Pt) are shown in Supporting Information (Figures S1−S4). Values of $<d_{TEM}>$ and $<d_{chem}>$ are in excellent agreement for metal clusters <1 nm in diameter (Table 1), however, d_{TEM} is larger than d_{chem} for 2.7 nm Ir clusters, perhaps because TEM overlooks a significant number of very small (<0.3 nm) clusters.

2.3. Catalytic Rates and Selectivities. Catalytic reactions were carried out in a packed-bed held within a stainless steel tube (3/8" O.D.) and accurately described by plug-flow hydrodynamics. This tubular reactor was placed within a three-zone resistively heated furnace; the bed temperature was held constant using temperature controllers (Watlow, 96) and measured with a type K thermocouple held within a coaxially aligned 1/16 in. stainless steel sheath within the bed. The catalysts were mixed with additional SiO_2 (Cab-O-Sil HS-5, washed with deionized water and treated in flowing dry air at

dx.doi.org/10.1021/ja4093743 | J. Am. Chem. Soc. 2013, 135, 18586−18599

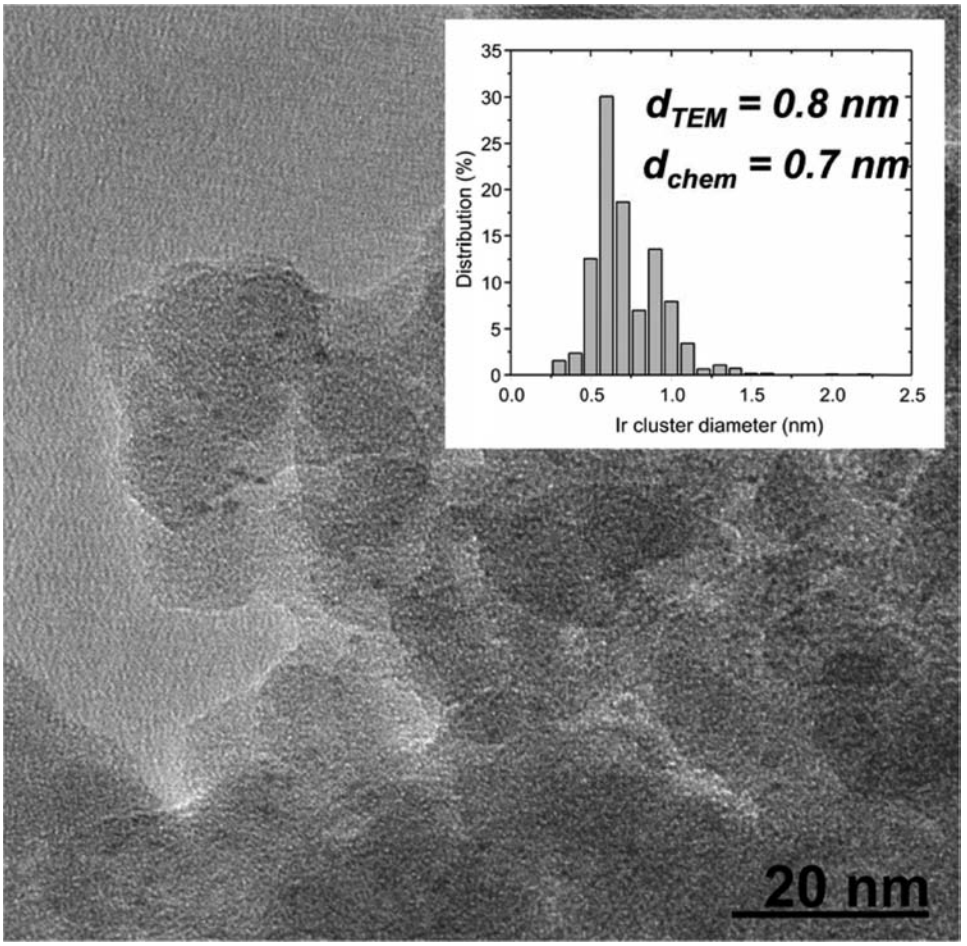

Figure 1. Representative image and cluster size distribution of 0.7 nm Ir−SiO_2 as obtained by transmission electron microscopy, 1234 clusters were counted to determine $<d_{TEM}>$, the surface-averaged diameter.

793 K for 5 h) to avoid axial or radial temperature gradients. The reactor pressure was controlled using a dome-loaded pressure regulator (Mity-Mite, S91XW).

Catalysts were treated in flowing H_2 (Praxair, 99.999%, 50 cm^3 g^{-1} s^{-1}) at ambient pressure by heating to 673 at 0.083 K s^{-1} and holding for 2 h before all catalytic measurements. H_2 (Praxair, 99.999%), ethane (5% ethane, 10% Ar, 85% He, Praxair, certified grade), propane (10% propane, 5% Ar, 85% He, Praxair, certified grade), and *n*-butane (10% n-butane, 5% Ar, 85% He, Praxair, certified-grade) were metered using mass flow controllers (Parker, 201). Liquid hydrocarbons (*n*-hexane, Alfa-Aesar, 99%; *n*-octane, Sigma-Aldrich, analytical grade; *n*-decane, Sigma-Aldrich, analytical grade) were introduced using a high-pressure syringe pump (Isco, 500D). Transfer lines, before and after the reactor, were maintained at ∼423 K to prevent condensation of reactants or products.

Molecular speciation of all streams was carried out by gas chromatography (Agilent GC, 5890) using a methyl silicone capillary column (HP-1, 50 m × 0.32 mm ×1.05 μm) and flame ionization detection. Standard compounds and an isoparaffin mixture (Sigma-Aldrich) were used for assigning chromatographic features; assignments were confirmed by mass spectrometry (Agilent, 5975C). All rates are reported at <10% reactant conversions to measure primary reactions and to ensure differential conditions. Turnover rates are reported as moles of carbon converted per unit time normalized by the number of surface metal atoms. Stated uncertainties are equivalent to two-standard deviations, i.e., 95% confidence intervals. Hydrogenolysis selectivities are reported as ratios of turnover rates for forming different products and are normalized by the number of C−C bonds present in the reactant that could cleave to form each product.

3. RESULTS AND DISCUSSION

3.1. Mechanistic Interpretation of Kinetics and Reactive Species Compositions. Figure 2 shows turnover rates for the cleavage of $^1C-^1C$ bonds in ethane (superscript denotes the number of alkyl groups bonded to the C-atom), $^2C-^1C$ bonds in propane, and all $^2C-^2C$ and $^2C-^1C$ bonds in C_4-C_{10} *n*-alkanes as a function of H_2 pressure (0.1−5.5 MPa; 20 kPa alkane; 593 K) on 0.7 nm Ir clusters. Alkane hydrogenolysis turnover rates depend on alkane and H_2 pressures, which determine the number and degree of unsaturation of the reactive and unreactive chemisorbed species.[3,10,17,45] At low H_2 pressures, *n*-alkane hydrogenolysis rates increase with increasing H_2 pressure (e.g., *n*-hexane, *n*-octane, Figure 2 (a)), because of a concomitant increase in the H-content of the pool of adsorbed hydrocarbons. These data indicate that the specific chemisorbed species that cleave the C−C bond contain a larger number of H-atoms than the average number of H-atoms present within all adsorbed species. Turnover rates ultimately reach maximum values and then decrease with increasing H_2 pressure because chemisorbed species become more saturated than the intermediates that lead to C−C bond cleavage. At these higher H_2 pressures, chemisorbed hydrogen atoms (H*) replace hydrocarbon-derived species as the most-abundant surface intermediates (MASI). Figure 2 (b) shows that ethane and *n*-hexane hydrogenolysis turnover rates on 0.9 nm Rh and 0.6 nm Pt clusters depend on the H_2 pressure in ways that are

dx.doi.org/10.1021/ja4093743 | J. Am. Chem. Soc. 2013, 135, 18586−18599

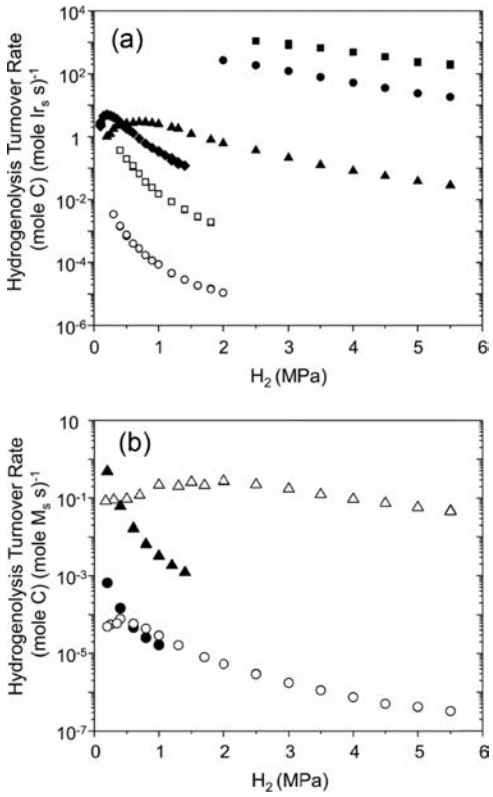

Figure 2. (a) Turnover rates of alkane conversion for ethane (○), propane (□), *n*-butane (♦), *n*-hexane (▲), *n*-octane (●), and *n*-decane (■) as a function of H_2 pressure on 0.7 nm Ir clusters at 20 kPa alkane, 593 K. (b) Turnover rates for alkane hydrogenolysis as a function of H_2 pressure on 0.6 nm Pt clusters (ethane, 653 K (●); and *n*-hexane, 593 K (○)) and on 0.9 nm Rh clusters (ethane, 593 K (▲); and *n*-hexane, 573 K (Δ)) at 20 kPa alkane.

Scheme 1. Proposed Intermediate Reactions for Hydrogenolysis of *n*-Alkanes on Supported Metal Clusters[a]

$$H_2 + 2\,* \overset{K_{H2}}{\rightleftharpoons} 2\,H^* \quad (1.1)$$

$$C_nH_{2n+2} \overset{K_{D,z}}{\rightleftharpoons} C_nH_{2n+2-z} + z\,½H_2 \quad (1.2)$$

$$C_nH_{2n+2-z} + 2\,* \overset{K_{A,z}}{\rightleftharpoons} {}^*C_nH_{2n+2-z}{}^* \quad (1.3)$$

$${}^*C_nH_{2n+2-y}{}^* \xrightarrow{k_R} C_aH_{a'}{}^* + C_{n-a}H_{2n+2-y-a'}{}^* \quad (1.4)$$

$$C_aH_{a'}{}^* + xH\,* \overset{K_{H,D}}{\rightleftharpoons} C_aH_{2a+2} + (x+1)^* \quad (1.5)$$

[a] * is an unoccupied surface site; the arrows denote a quasi-equilibrated step; k_x and K_x are kinetic and equilibrium constants, respectively, for each reaction; and the reactive intermediate (C_nH_{2n+2-y}) are a subset of the pool of the quasiequilibrated pool of hydrogen-deficient intermediates (C_nH_{2n+2-z}) such that $y \leq z$.

consistent with the behavior and chemical interpretation of alkane and H_2 reactants on Ir clusters (Figure 2 (a)).

Scheme 1 shows a sequence of elementary steps consistent with the observed kinetic effects of the alkane and H_2 pressures (Figure 2) on hydrogenolysis turnover rates on metal clusters:[46−48]

In this scheme, (*) denotes exposed metal atoms, and X* and *X* are α-coordinated and α,β-coordinated intermediates, respectively. H_2 dissociation (1.1) and all hydrogenation−dehydrogenation (1.2) and adsorption−desorption (1.3) steps are assumed to be quasi-equilibrated and to form a pool of H-deficient adsorbed species (C_nH_{2n+2-z}, z is the number of H-atoms removed from each alkane). These equilibrium assumptions were confirmed for cycloalkanes and isoalkanes, for which the respective alkenes are detectable, at similar conditions.[46,47] Equilibrium *n*-alkene concentrations are below detection limits at the conditions of our experiments (10^{-5}−10^{-4} Pa alkenes),[49] but quantum chemical calculations show that on Ir forward and reverse barriers to remove up to four H-atoms from ethane are less, by 60 kJ mol^{-1}, than barriers to cleave the C−C bond, indicating that dehydrogenation steps are quasi-equilibrated.[46]

Quasi-equilibrated H−H and C−H bond activation steps precede kinetically relevant C−C bond cleavage steps (1.4)[47] in α,β-coordinated reactive intermediates with a given H-content (${}^*C_nH_{2n+2-y}{}^*$, y is the number of H-atoms removed from the *n*-alkane reactant to form the reactive intermediate); these intermediates exist as part of the equilibrated pool of H-deficient intermediates. Transition-state theory assumes that the activated complex that cleaves the C−C bond exists in hypothetical equilibrium with the H-deficient reactive intermediates.[50] C−C bond cleavage forms two hydrocarbon fragments ($C_aH_{a'}{}^*$ and $C_bH_{b'}{}^*$) bound to the surface through their terminal C-atoms, and these fragments hydrogenate and desorb as smaller alkanes in subsequent quasi-equilibrated steps (1.5).

Scheme 1 leads to hydrogenolysis rates proportional to the concentration of the reactive unsaturated intermediate ([${}^*C_nH_{2n+2-y}{}^*$])

$$r = k_R \cdot [{}^*C_nH_{2n+2-y}{}^*] \quad (2)$$

in which k_R is the C−C bond cleavage rate constant. The pseudo-steady-state hypothesis (PSSH) for [${}^*C_nH_{2n+2-y}{}^*$] species leads to the rate equation

$$r = k_R K_{D,y} K_{A,y} (P_{RH})(P_{H_2})^{-y/2} \cdot \frac{[*]^2}{[L]} \quad (3)$$

in terms of H_2 and alkane (RH) pressures (P_{H2}, P_{RH}). This equation contains equilibrium constants for alkane dehydrogenation ($K_{D,y}$) and for adsorption of species with y H-atoms removed from the alkane ($K_{A,y}$). Here, [*] denotes the number of unoccupied sites and [L] the total number of active surface sites, which is equal to the number of M_s atoms. Equation 3 depends on [*]^2 because α,β-coordinated reactive species occupy two vicinal sites (*−*)[3] and the C−C cleavage fragments each require one site for binding.[48,51] The full rate equation has a complex form (shown in the Supporting Information) that precludes direct chemical interpretations of turnover rate measurements; however, this equation becomes much simpler when H* or alkane-derived species become the MASI.

At low H_2/RH reactant ratios, cluster surfaces become covered by an equilibrated pool of alkane-derived species [${}^*C_nH_{2n+2-z}{}^*$], with z values set by the prevalent H_2 pressure and by the values of $K_{D,z}$ and $K_{A,z}$, which reflect homolytic C−H and metal−carbon (M−C) bond dissociation energies, respectively. In this case, eq 3 becomes

dx.doi.org/10.1021/ja4093743 | J. Am. Chem. Soc. 2013, 135, 18586−18599

$$\frac{r}{[L]} = k_R \cdot \frac{K_{D,y}K_{A,y}(P_{RH})(P_{H_2})^{-y/2}}{(\sum_{z=1}^{2n+2} K_{D,z}K_{A,z}(P_{RH})(P_{H_2})^{-z/2})} = k_R \cdot \frac{K_{D,y}K_{A,y}(P_{H_2})^{-(y-z_{eff})/2}}{K_{D,z_{eff}}K_{A,z_{eff}}} \quad (4)$$

in which z_{eff} represents the average number of H-atoms removed from alkanes to form the pool of equilibrated species, and $K_{D,z_{eff}}$ and $K_{A,z_{eff}}$ are effective equilibrium constants for the dehydrogenation of the alkane to the pool of H-deficient species and for their chemisorption on cluster surfaces, respectively. Equation 4 is consistent with hydrogenolysis rates that increase with H_2 pressure at low H_2 pressures (Figure 2 (a, b)), for which the mean H-content of alkane-derived intermediates is less than in the intermediate that cleaves C−C bonds ($z_{eff} > y$). Equation 4 is also consistent with hydrogenolysis rates that are independent of alkane pressure when alkane-derived intermediates are the MASI.[47] The lumped nature of the kinetic and thermodynamic terms in eq 4 precludes a more precise mechanistic analysis from rate data measured in this kinetic regime. Only differences between y and z_{eff} are measurable, making the nature of the reactive species ($^*C_nH_{2n+2-y}^*$), the composition of the surface pool ($^*C_nH_{2n+2-z}^*$), and the relevant equilibrium constants ($K_{D,y}$, $K_{A,y}$, $K_{D,z_{eff}}$, and $K_{A,z_{eff}}$) inaccessible to experimental verification.

A more rigorous and precise mechanistic analysis becomes possible, however, at high H_2/RH reactant ratios, when H* is the MASI and eq 3 becomes

$$r = k_R \cdot \frac{K_{D,y}K_{A,y}(P_{RH})}{K_{H_2}(P_{H_2})^{y+2/2}} \cdot [L] \quad (5)$$

This equation allows the effects of H_2 pressure on rates to be used to determine the number of H-atoms (y) that must be removed from the alkane to form the intermediate that cleaves the C−C bonds. Equation 5 is consistent with the observed decrease in rates with increasing H_2 pressure (Figure 2 (a, b)) and with the linear dependence of hydrogenolysis rates on n-alkane,[48] isoalkane,[46] and cycloalkane pressures at high H_2/RH ratios.[47]

The mechanistic interpretation of eq 5 allows hydrogenolysis rates to be expressed in terms of the rate constant for cleaving the C−C bond in the reactive intermediate and the equilibrium constants for forming the specific intermediate that undergoes C−C bond cleavage, without needing to consider the entire pool of H-deficient species. This, however, requires experimental verification that H* is indeed the MASI and that y is invariant with H_2 pressure. These requirements do not appear to have consistently been met in previous studies, as reported by Bond[3] and references therein.

The data in Figure 2 (a, b) show that hydrogenolysis rates are accurately described by

$$r = A \cdot \frac{P_A}{P_{H_2}^{\lambda}} \quad (6)$$

at high H_2 pressures. Here, λ equals $(y + 2)/2$ and A is the product of the lumped rate and equilibrium constants in eq 5:

$$A = \frac{k_R K_{D,y} K_{A,y}}{K_{H_2}} \quad (7)$$

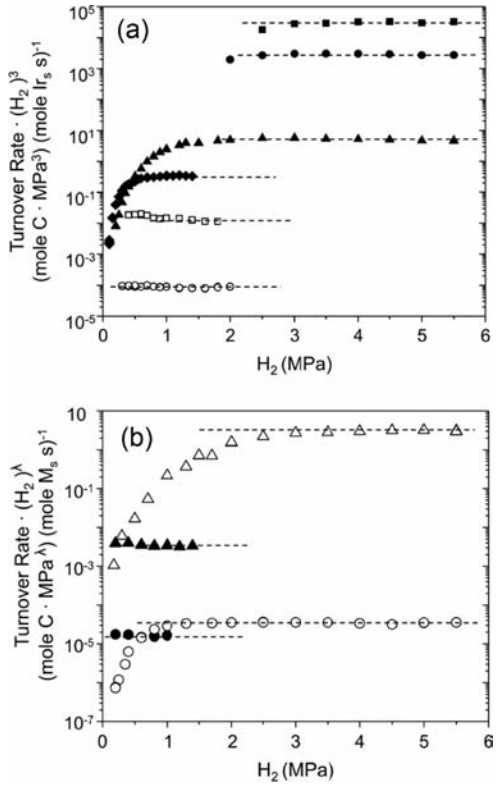

Figure 3. (a) Hydrogenolysis turnover rates multiplied by H_2 pressure cubed for ethane (○), propane (□), n-butane (♦), n-hexane (▲), n-octane (●), and n-decane (■) as a function of H_2 pressure on 0.7 nm Ir clusters at 20 kPa alkane, 593 K. This linearized form shows that the decrease in n-alkane hydrogenolysis turnover rates follow an inverse cubic dependence on H_2. (b) Hydrogenolysis turnover rates multiplied by H_2 pressure to the λ power showing that n-alkane hydrogenolysis turnover rates decrease with a constant dependence on H_2 at 20 kPa alkane on 0.6 nm Pt clusters for ethane (λ = 2.3, 653 K (●)) and n-hexane (λ = 2.8, 593 K (○)) and on 0.9 nm Rh clusters for ethane (λ = 3.0, 593 K (▲)) and n-hexane (λ = 2.3, 573 K (Δ)).

Measured rates (Figure 2; 0.7 nm Ir clusters) are consistent with a λ of 3.0 ± 0.2 for all n-alkanes. This is shown by the data in Figure 3 (a), in which rates multiplied by $(P_{H2})^3$ reach constant values at high H_2 pressures for all n-alkanes. These data indicate that all n-alkanes (C_2−C_{10}) lose four H-atoms (y = 4.0 ± 0.3) to form the intermediate that undergoes C−C bond cleavage. The specific structure of these reactive species cannot be determined more precisely from these data, but the tendency of C-atoms to adopt tetrahedral coordinations[52] and the enthalpic preference for M−C bonds[52] over the sp or sp^2 hybridizations of C≡C or C═C bonds[53] suggest that one M−C bond replaces each H-atom removed from the alkane. Entropy considerations indicate that conformational freedom in chemisorbed hydrocarbons favors the formation of surface attachments at vicinal C-atoms, making it likely that all four M−C bonds form at adjacent C-atoms to give α,β-bound intermediates with tetra-σ or di-σ/π bonds to the cluster surface.[3,54,55]

Figure 3 (b) confirms that C−C bond cleavage on 0.9 nm Rh clusters and 0.6 nm Pt clusters occurs in similarly dehydrogenated reactive intermediates for ethane (y = 4.0 ± 0.6 (Rh) and 2.6 ± 0.6 (Pt)) and n-hexane (y = 2.6 ± 0.4 (Rh) and 3.5 ± 0.4 (Pt)). Yet, the compositions of reactive intermediates differ among Ir, Rh, and Pt because differences between C−C and

dx.doi.org/10.1021/ja4093743 | J. Am. Chem. Soc. 2013, 135, 18586−18599

C−H bond activation energies on each metal cause C−C bond cleavage to occur after fewer H-atoms have been removed from alkanes on Rh and Pt.

C−C bonds can cleave at nonterminal (NT, ^{2}C−^{2}C) or terminal (T, ^{2}C−^{1}C) positions in *n*-alkanes; these positions differ in the substitution of the C-atoms involved. C−C bond cleavage selectivities are defined here as

$$\beta_{NT-T} = \frac{(r_{NT}/\sigma_{NT})}{(r_T/\sigma_T)} \quad (8)$$

where r_{NT} and r_T are the rates of C−C bond rupture at nonterminal and terminal positions, respectively, while σ_{NT} and σ_T represent the number of nonterminal and terminal C−C bonds in a given alkane. The effects of H_2 pressure on β_{NT-T} (Figure 4) depend on differences in the extent of

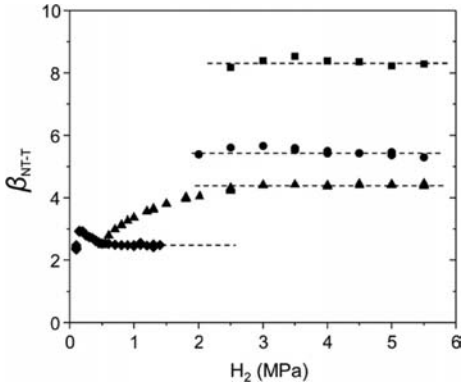

Figure 4. Location of C−C bond cleavage in *n*-butane (♦), *n*-hexane (▲), *n*-octane (●), and *n*-decane (■) as a function of H_2 pressure on 0.7 nm Ir clusters at 20 kPa alkane, 593 K. β_{NT-T} is the ratio of turnover rates for nonterminal and terminal C−C bond hydrogenolysis normalized by the statistical occurrence of the bonds within the reactant.

dehydrogenation of the intermediates that cleave C−C bonds at terminal and nonterminal positions:

$$\beta_{NT-T} = \frac{\sigma_T}{\sigma_{NT}} \cdot \frac{A_{NT} P_{H_2}^{\lambda_T}}{A_T P_{H_2}^{\lambda_{NT}}} \quad (9)$$

Here, the constants (A_{NT} and A_T) for C−C bond cleavage are given by the respective values of A (eq 7) for each C−C bond position on H*-covered Ir surfaces (eq 5; H* as MASI). The β_{NT-T} values for C_4−C_{10} *n*-alkanes do not depend on H_2 pressure on H*-saturated Ir clusters (Figure 4), indicating that the alkane-derived species that form kinetically relevant transition states for hydrogenolysis of ^{2}C−^{1}C or ^{2}C−^{2}C bonds in a given *n*-alkane contain an identical number of H-atoms.

3.2. Activation Enthalpies and Entropies for *n*-Alkane Hydrogenolysis. The kinetic response of hydrogenolysis rates to H_2 (Figure 2) and alkane pressures[46,48,56,57] indicates that all steps preceding C−C bond cleavage are quasi-equilibrated. For all kinetic regimes and surface coverages, *α,β*-bound reactive species remain quasi-equilibrated with gaseous H_2 and *n*-alkane reactants, as shown by the facile equilibration of cycloalkane−arene[47] and isoalkane−isoalkene[46] mixtures at similar conditions and by theoretical estimates that show forward and reverse barriers for C−H bond cleavage are much less than those for C−C bond cleavage in ethane derived surface intermediates on Ir.[48]

Transition-state theory invokes a hypothetical equilibrium between reactants and activated complexes[50] in elementary steps; in this case, this requires that the transition state be also equilibrated with gaseous alkane reactants, as shown in Scheme 2. The lumping of all equilibrated elementary steps leading to the transition state that mediates the cleavage of the C−C bond (1.4) on H*-covered Ir surfaces, reflected in the functional form of eq 5, gives the overall stoichiometric reaction:

$$C_nH_{2n+2} + 2H^* \overset{K'^{\ddagger}}{\rightleftharpoons} {}^*C_nH_{2n+2-2\lambda}{}^{*\ddagger} + \lambda H_2 \quad (10)$$

Here, $K'^{\ddagger}$ is the equilibrium constant for the formation of the transition state ($^*C_nH_{2n-2}{}^{*\ddagger}$) and λ H_2 molecules (λ = 3 on 0.7 nm Ir (Scheme 2) but is between 2.3 and 3.0 for ethane and hexane on Rh and Pt clusters, Table S1, Supporting Information) by dehydrogenating the gaseous alkane and desorbing two H* to form the *−* site pair required to bind the transition state on H*-covered surfaces. Thus, on 0.7 nm Ir, eq 10 takes the form C_nH_{2n+2} + 2H* $\overset{K'^{\ddagger}}{\rightleftharpoons}$ $^*C_nH_{2n-2}{}^{*\ddagger}$ + $3H_2$. Then, hydrogenolysis turnover rates given by transition-state theory are equal to the concentration of the activated complexes multiplied by the frequency at which they cleave the C−C bond[50]

$$\frac{r_{RH}}{[L]} = \nu^{\ddagger}[{}^*C_nH_{2n+2-y}{}^{*\ddagger}] = \nu^{\ddagger}K'^{\ddagger}\frac{P_{RH}}{P_{H_2}^{\lambda}} \quad (11)$$

where the vibration along the reaction coordinate, $\nu^{\ddagger}$, corresponds to the weak vibration of the C−C bond being cleaved. Canceling $\nu^{\ddagger}$with the partition function for the weak C−C bond stretch at the transition state ($\sim((k_BT)/(h\nu^{\ddagger}))$ for weak vibrations) gives

$$\frac{r_{RH}}{[L]} = \frac{k_BT}{h}\cdot K^{\ddagger}\cdot\frac{P_{RH}}{P_{H_2}^{\lambda}} = \frac{k_BT}{h}\cdot e^{-\Delta G^{\ddagger}/RT}\cdot\frac{P_{RH}}{P_{H_2}^{\lambda}} \quad (12)$$

where k_B and h are the Boltzmann and Planck constants, respectively, and $K^{\ddagger}$ is the transition-state equilibrium constant (calculated from partition functions for the activated complex which exclude the C−C bond stretch). This $K^{\ddagger}$ value reflects the free energy of activation ($\Delta G^{\ddagger}$), which contains the additive contributions of all preceding steps.

The path-independent properties of state functions, such as free energies, allow $\Delta G^{\ddagger}$ to be expressed in terms of a hypothetical sequence of steps, chosen to include steps with thermodynamic properties that are tabulated or accessible to statistical mechanics formalisms.[49] The sequence of reactions in Scheme 1 can be described by such a Born−Haber thermochemical pathway, which includes free energy changes associated with alkane dehydrogenation to form the gaseous analogue of the dehydrogenated reactive intermediate (1.2, ΔG_D), the recombinative desorption of two H* from the surface (1.1, ΔG_{H2}), and the adsorption of the gaseous analogue of the reactive dehydrogenated alkane on *−* (1.3, ΔG_A). Subsequently, the transition state forms (1.4, ΔG_R) and the C−C bond cleaves.

Scheme 2 shows changes in free energy for a hypothetical reaction pathway on H*-covered metal surfaces and its corresponding $\Delta G^{\ddagger}$:

$$\Delta G^{\ddagger} = G^{\ddagger} + \lambda\cdot G_{H2} - 2G_{H^*} - G_{RH} \quad (13)$$

This equation contains free energies for the transition state ($G^{\ddagger}$), for λ (equal to 3 in Scheme 2) gaseous H_2 molecules (G_{H2}), for

dx.doi.org/10.1021/ja4093743 | J. Am. Chem. Soc. 2013, 135, 18586−18599

Scheme 2. Changes in Free Energy Due to the Intermediate Reactions That Form the Transition State (Shown for Central Bond Cleavage in *n*-Hexane) for C−C Bond Rupture Beginning with a Gas-Phase Alkane and a H*-Covered Ir Surface[a]

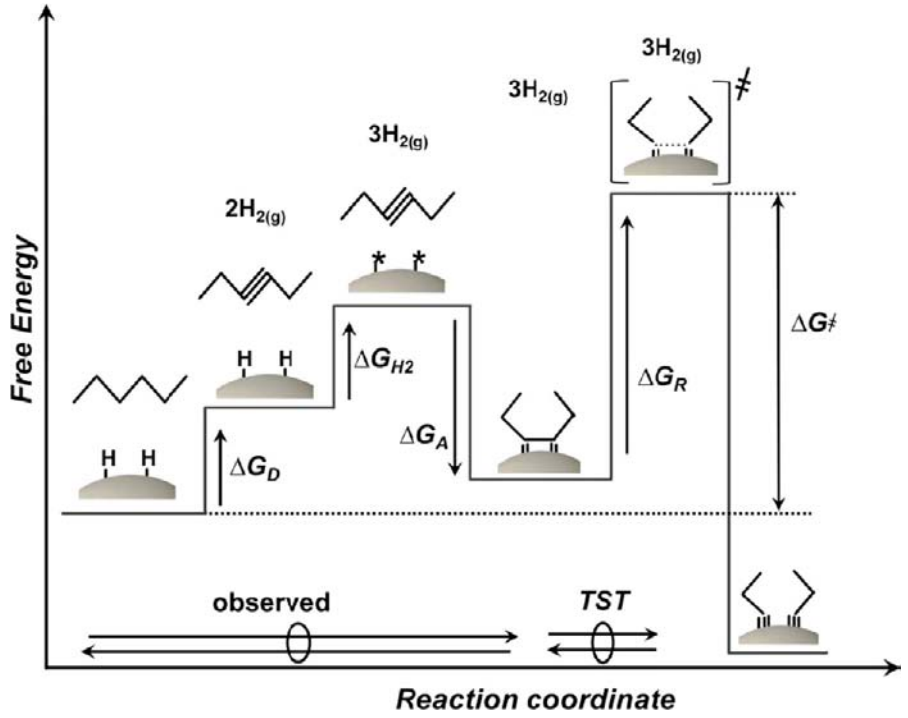

[a]For this example, the value of λ from eq 13 is 3. The free energy of activation ($\Delta G^{\ddagger}$) is given by the sum of the free energies of dehydrogenation (ΔG_{D}), hydrogen desorption (ΔG_{H2}), adsorption of the dehydrogenated hydrocarbon (ΔG_{A}), and the formation of the transition state from the reactive intermediate (ΔG_{R}). Free energies of intermediate species cancel such that $\Delta G^{\ddagger}$ (eq 13) is given by the difference between the free energies of the reactants (hexane and 2H*) and the "products" (the transition state and $3H_2(g)$) in the stoichiometric reaction that forms the C−C cleavage transition state (eq 10).

the two H* (G_{H*}) that must desorb to accommodate the transition state, and for the gaseous alkane reactant (G_{RH}). $\Delta G^{\ddagger}$ is calculated using the turnover rate (as alkane molecules per surface metal atom per unit time) measured at each temperature (eq 12). Changes in $\Delta G^{\ddagger}$ with reciprocal temperature give the activation enthalpy ($\Delta H^{\ddagger}$) and entropy ($\Delta S^{\ddagger}$) for cleaving the C−C bond, which also reflect the respective additive contributions from each hypothetical step in the thermochemical cycle (Scheme 2):

$$\Delta H^{\ddagger} - T\Delta S^{\ddagger} = (H^{\ddagger} + \lambda \cdot H_{H2} - 2H_{H*} - H_{RH}) - T(S^{\ddagger} + \lambda \cdot S_{H2} - 2S_{H*} - S_{RH}) \quad (14)$$

Figure 5 shows $K^{\ddagger}$ values determined from measured turnover rates for the cleavage of $^{2}C-^{2}C$ and $^{2}C-^{1}C$ bonds in n-butane, *n*-hexane, *n*-octane, and *n*-decane and for the cleavage of $^{2}C-^{1}C$ and $^{1}C-^{1}C$ bonds in propane and ethane, respectively, as a function of reciprocal temperature. Turnover rates were measured at high H_2/RH ratios (60−175) to ensure that surfaces remained saturated with H* at all temperatures. Table 2 shows $\Delta H^{\ddagger}$ and $\Delta S^{\ddagger}$ values and their 95% confidence intervals for hydrogenolysis of C_2-C_{10} *n*-alkanes on 0.7 nm Ir clusters. $\Delta H^{\ddagger}$ and $\Delta S^{\ddagger}$ values for ethane and *n*-hexane on the surfaces of 1.3 nm Ir, 2.7 nm Ir, 0.9 nm Rh, and 0.6 nm Pt clusters are shown in the Supporting Information (Table S1).

Measured $\Delta H^{\ddagger}$ values on 0.7 nm Ir clusters are largest for ethane (257 ± 2 kJ mol^{-1} K^{-1}) and decrease monotonically with increasing *n*-alkane size, reaching constant values for C_6-C_{10} (216 ± 4 kJ mol^{-1} K^{-1}). The value of $\Delta H^{\ddagger}$ for $^{1}C-^{1}C$ bond cleavage in ethane is larger than for $^{2}C-^{1}C$ bond cleavage

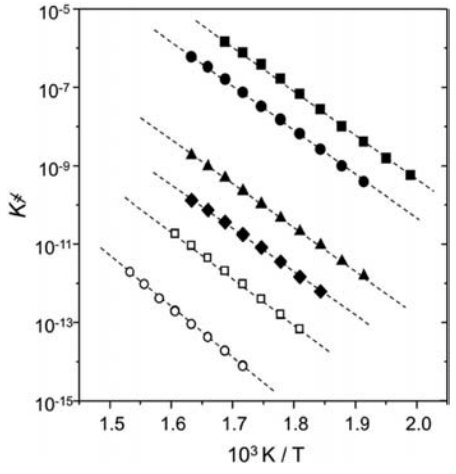

Figure 5. Eyring−Polanyi plots of apparent rate constants for hydrogenolysis of alkanes: ethane (○), propane (□), *n*-butane (♦), *n*-hexane (▲), *n*-octane (●), and *n*-decane (■) on hydrogen-covered surfaces of 0.7 nm Ir clusters at 20 kPa alkane.

in propane (by 27 kJ mol^{-1}) and for $^{2}C-^{2}C$ and $^{2}C-^{1}C$ bond cleavage in longer *n*-alkanes (by 40 kJ mol^{-1}). $\Delta H^{\ddagger}$ values for ethane are consistently 20−50 kJ mol^{-1} larger than for the $\Delta H^{\ddagger}$ for *n*-hexane, and this difference persists independent of cluster size (0.7 nm, 1.3 nm, and 2.7 nm Ir clusters) or metal identity (0.7 nm Ir, 0.9 nm Rh, and 0.6 nm Pt clusters) (Table S1, Supporting Information). These different enthalpies reflect, in part, concomitant differences in homolytic C−C bond dissociation energies (BDE(C−C)), which decrease with increasing

dx.doi.org/10.1021/ja4093743 | J. Am. Chem. Soc. 2013, 135, 18586−18599

Table 2. Activation Enthalpies (kJ mol^{-1}) and Entropies (J mol^{-1} K^{-1}) for *n*-Alkane Hydrogenolysis on 0.7 nm Ir Clusters at 593 K

reactant alkane	$\Delta H^{\ddagger a}$	$\Delta S^{\ddagger a}$	$S_{H_2}{}^{b,c}$	$S_{RH}{}^{b}$	$2S_{A,H}{}^{d}$	experimental $S^{\ddagger e}$
ethane	257 ± 3	171 ± 5	138	289	72	118 ± 5
propane	230 ± 3	164 ± 5	138	345	72	167 ± 5
n-butane	228 ± 2	186 ± 6	142	403	72	235 ± 6
n-hexane	217 ± 3	170 ± 5	133	510	72	353 ± 5
n-octane	219 ± 4	240 ± 6	133	616	72	528 ± 6
n-decane	214 ± 5	259 ± 9	133	741	72	673 ± 9

[a]Measured value from Eyring–Polanyi plot. [b]Calculated entropies of gas-phase species from published partition functions.[59] [c]Changes in S_{H2} reflect differences between H_2 pressures used for each *n*-alkane. [d]Calculated assuming a two-dimensional ideal gas at 593 K and $H/Ir_s = 1$. [e]Determined using eq 15.

substitution at the C-atoms in a given C–C bond in alkanes. For example, tabulated BDE(C–C) values show that the ^{1}C–^{1}C bond in ethane is 19 ± 4.2 kJ mol^{-1} stronger than ^{2}C–^{1}C bonds in C_3–C_6 *n*-alkanes and 35 ± 4.2 kJ mol^{-1} stronger than ^{2}C–^{2}C bonds in C_4–C_6 *n*-alkanes.[53] Figure 6

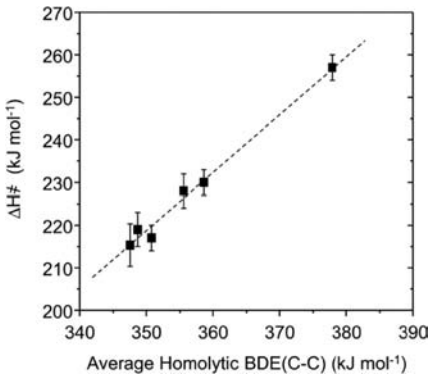

Figure 6. Correlation between average homolytic C–C bond dissociation energy, BDE(C–C), and activation enthalpies, $\Delta H^{\ddagger}$, for hydrogenolysis of *n*-alkanes on hydrogen-covered surfaces of 0.7 nm Ir clusters at 20 kPa of *n*-alkane. Average BDE(C–C) values were determined by averaging the gas-phase homolytic BDE(C–C) values for distinct C–C bonds within each *n*-alkane.[53]

shows that $\Delta H^{\ddagger}$ for hydrogenolysis of *n*-alkanes on H*-covered Ir clusters reflect differences in their BDE(C–C) values (averaged over all C–C bonds).[53] Yet, $\Delta H^{\ddagger}$ values for cleavage at the different C–C positions in a given *n*-alkane (C_4–C_{10}) are similar, suggesting that $\Delta H^{\ddagger}$ values for breaking ^{1}C–^{2}C and ^{2}C–^{2}C bonds depend also on factors other than BDE(C–C), such as steric repulsion effects,[58] which tend to destabilize transition states for ^{2}C–^{2}C bonds more than at terminal ^{1}C–^{2}C bonds. The similar $\Delta H^{\ddagger}$ values for *n*-hexane, *n*-octane, and *n*-decane reflect the weak effects of additional ^{2}C–^{2}C bonds on average BDE(C–C) values for *n*-alkanes.[53] Hydrogenolysis turnover rates differ by 10^8 between ethane and *n*-decane (593 K; Figure 2) as a consequence of concomitant differences in $K^{\ddagger}$ (Figure 5), which cannot solely reflect relatively small changes in $\Delta H^{\ddagger}$ with chain length. ($K^{\ddagger}$ values are defined per mole alkane and therefore do not artificially increase values of $K^{\ddagger}$ for longer *n*-alkanes, which would occur if rates were define per mole carbon.) We conclude, as a result, that such reactivity differences must reflect strong effects of chain length on hydrogenolysis $\Delta S^{\ddagger}$ values.

$\Delta S^{\ddagger}$ values for C–C bond cleavage in *n*-alkanes (Table 2; 0.7 nm Ir clusters) are large and positive (164–259 J mol^{-1} K^{-1}), consistent with large entropic gains in forming the transition state, which result from the evolution of three H_2 molecules (4 H-atoms from the alkane and two H* desorbed to bind the transition state) from the relevant reactant state (eq 10). Ethane and *n*-hexane hydrogenolysis on Rh, Pt, and larger Ir clusters also exhibit large $\Delta S^{\ddagger}$ (Table S1, Supporting Information, 41–193 J mol^{-1} K^{-1}) that increase with the amount of H_2 produced (λ). These data show that hydrogenolysis represents a prototypical example of a chemical reaction with a high activation barrier and which is largely driven by large entropy gains in the equilibrated steps that form the transition state. These reactions overcome high enthalpic barriers (Table 2, 216–257 kJ mol^{-1}) for cleaving strong C–C bonds only as a result of the entropy gained by the evolution of H_2(g), by the quasi-equilibrated elementary steps that precede transition state formation, even though each overall hydrogenolysis event actually consumes one H_2(g) molecule. The functional form of $\Delta G^{\ddagger}$ ($\Delta H^{\ddagger} - T\Delta S^{\ddagger}$, eq 14) shows that entropy gains decrease $\Delta G^{\ddagger}$ more effectively as the temperature of the reaction increases.

The entropy of the transition state mediating C–C bond cleavage ($S^{\ddagger}$) can be estimated from measured activation entropies ($\Delta S^{\ddagger}$) by rearranging the terms in eq 14:

$$S^{\ddagger} = \Delta S^{\ddagger} - \lambda \cdot S_{H2} + 2 \cdot S_{H*} + S_{RH} \quad (15)$$

The entropy of H_2(g) (S_{H2}) can be estimated using statistical mechanics formalisms with partition functions for three-dimensional translation of ideal gases, rotation of rigid rotors, and harmonic oscillators.[59] At the temperatures of catalytic hydrogenolysis (500 – 700 K), H_2 adsorbs dissociatively and H* behaves as a two-dimensional ideal gas with one vibrational mode perpendicular to the metal surface (e.g., ν(Ir–H) = 2030 cm^{-1} on Ir(111)).[60] Activation entropies for hydrogenolysis are measured on H*-saturated surfaces; therefore, S_{H*} values were calculated for H/M_s coverages of unity from the relevant partition functions[61] and give an entropy of 36 J mol^{-1} K^{-1} for S_{H*} (i.e., 72 J mol^{-1} K^{-1} per mole H_2). S_{H*} values at saturation H* coverages are insensitive to the elemental identity of the metal cluster, because the identity of the surface metal atoms minimally influences the frequency of the vibrational mode perpendicular to the surface and the area for two-dimensional translation. Calculations for S_{RH} use partitions functions for three-dimensional translation, rigid rotors, and vibrations from normal modes obtained from coupled-cluster doubles (CCD) level of theory with the 6-31G* basis set.[62] These calculations give entropies that are 1–5% smaller than the tabulated data[49] for these gaseous species because such calculations neglect configurational entropies from trans, gauche–, and gauche+ rotational conformations about C–C bonds.[63] Thus, we choose to calculate $S^{\ddagger}$ from experiments using S_{RH} values determined from the partition functions described above so that comparisons between calculated and predicted $S^{\ddagger}$ values use similar partition functions (see below) for all species and are not subject to systematic bias by incorporating tabulated data only in calculations for gaseous alkanes and H_2.

Table 2 shows the entropies for all stable gaseous and surface species involved in alkane hydrogenolysis; these values, taken together with measured $\Delta S^{\ddagger}$ values, give the entropy for the C–C bond cleavage transition states (eq 15). These $S^{\ddagger}$ values increase sharply with increasing *n*-alkane chain length (by 555 J mol^{-1} K^{-1} between ethane and *n*-decane); notably, the

dx.doi.org/10.1021/ja4093743 | J. Am. Chem. Soc. 2013, 135, 18586–18599

increases in $S^{\ddagger}$ with chain length are larger than for the respective gaseous alkanes (S_{RH}, 452 J mol^{-1} K^{-1}). Thus, transition states for larger alkanes retain a larger fraction of the entropy (S_{RH}) of their gaseous precursors, largely in the form of intramolecular vibrations.[61] This accounts for the larger $\Delta S^{\ddagger}$ (Table 2) and the higher hydrogenolysis turnover rates (Figure 2 (a)) of longer chain *n*-alkanes. Similar effects also account for the difference in $\Delta S^{\ddagger}$ (Table S1, Supporting Information) and turnover rates (Figure 2 (b)) between ethane and *n*-hexane on Rh, Pt, and larger Ir clusters. Thus, hydrogenolysis rates increase with the chain length of *n*-alkane reactants because of ubiquitous entropy effects that do not depend on the size or identity of the metal clusters used as catalysts.

3.3. Statistical Mechanics Descriptions of Hydrogenolysis Transition-State Entropies ($S^{\ddagger}$). Differences in $\Delta S^{\ddagger}$ (Table 2) cause the large differences in hydrogenolysis turnover rates among *n*-alkanes (Figure 2). $\Delta S^{\ddagger}$ values can be estimated using statistical mechanics formalisms for the proposed α,β-bound transition-state structure (Figure 7).

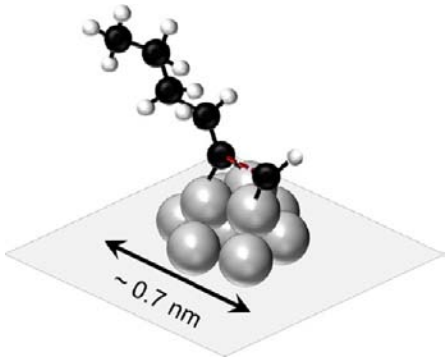

Figure 7. Schematic of the modeled transition state structure for hydrogenolysis of the terminal C−C bond in *n*-hexane on silica supported 0.7 nm (10 atom) metal clusters. The structure is depicted as being tetra-σ bound with α,β-coordination with all carbon atoms occupying tetrahedral bonding configuration. Alkyl chains are shown as all-trans conformers.

Metal-catalyzed C−C bond cleavage is exothermic (−30 to −200 kJ mol^{-1}) because two metal−carbon bonds (e.g., BDE(Pt−C) = 225−270 kJ mol^{-1})[64,65] form for each C−C bond cleaved (BDE(M−C) = 350− 439 kJ mol^{-1});[53] as a result, Hammond's postulate suggests that the C−C bond cleavage transition state occurs early along the reaction coordinate and resembles its α,β-bound reactive precursor.[66] Thus, we propose a transition state for terminal C−C hydrogenolysis in *n*-hexane (Figure 7, for metal clusters <1 nm in diameter, depicted as a 10-atom truncated cuboctahedron) similar in structure to the α,β-bound hydrocarbons detected spectroscopically on metal surfaces.[67,68] Such structures contain alkyl chains at each of the two C-atoms in the α,β-bound C−C unit; its configuration preserves the bond lengths and angles of the gaseous analogs in every part of the complex (0.109 nm C−H and 0.154 nm C−C bonds; 109.5° H−C−H and C−C−C bond angles).[69,70]

The partition function for these complexes is given by the product of the those for two-dimensional (surface) translation ($q_{t,2D}$), vibrations (q_v), and one-dimensional rotation ($q_{r,1D}$) and for rotational conformations about each of the C−C bonds (q_c):

$$q = q_{t,2D} q_v q_{r,1D} q_c \tag{16}$$

The translational partition function for strongly bound hydrocarbons reflects their frustrated motion parallel to the surface, treated as harmonic oscillations, which is described by two degenerate vibrational modes[59]

$$q_{t,2D} = \left(\frac{1}{1 - e^{-h\nu_t / k_B T}} \right)^2 \tag{17}$$

where the frequency (ν_t) is the same for the two modes because of the isotropic nature of the potential energy surface[59]

$$\nu_t = \left(\frac{E_d}{2md_M^2} \right)^{1/2} \tag{18}$$

where the mass (m) is that of the transition state complex; d_M is the M−M distance at the surface (e.g., d_{Ir} = 0.25 nm),[70] and E_d is the barrier for surface diffusion, which is taken as 46 kJ mol^{-1}, by analogy with values reported for methyl groups chemisorbed on Ir(111).[71]

The vibrational partition function (q_v) consists of those for each independent vibration (q_{vi}) at the transition state

$$q_v = \prod_i \frac{e^{-h\nu_i / 2k_B T}}{1 - e^{-h\nu_i / k_B T}} \tag{19}$$

where ν_i is the frequency of the ith vibrational mode. These modes are assumed to be identical in the transition state and the gaseous alkanes (obtained from coupled-cluster doubles (CCD) level of theory with the 6-31G* basis set),[62] except that the transition state excludes the ν(C−C) mode corresponding to the reaction coordinate[50] and the four ν(C−H) modes lost from abstracting the four H-atoms from the surface-bound carbon atoms. Vibrational modes include stretching, bending and deformation, as well as hindered rotations of methylene and methyl units within chains. Vibration normal to the surface corresponds to a ν(C−Ir) like mode with a frequency assumed to be 491 cm^{-1}, by analogy with those reported for methyl groups at on-top sites on Ir(111).[71]

The one-dimensional rotational partition function, $q_{r,1D}$, describes rotation about the surface normal by the two pendant alkyl chains attached to the α and β C-atoms bound to the surface (Figure 7). This motion is described as a rigid rotor[59]

$$q_{r,1D} = \left(\frac{8\pi^3 k_B T \cdot I_z}{h^2} \right)^{1/2} \tag{20}$$

in which I_z is the moment of inertia about the normal axis of rotation. Each alkyl chain is assumed to rotate freely and independently, but steric and electronic interactions with surfaces or vicinal adsorbates may well hinder rotation and decrease $q_{r,1D}$.[59] The moment of inertia (I_z) for each alkyl chain[59]

$$I_z = \sum_{i=1}^{l} m_i \cdot r_i^2 \tag{21}$$

reflects the mass (m_i) and distance from the rotational axis (r_i) for each C- and H-atom in the alkyl chain (total number, l). Alkyl chains have C−C and C−H bond lengths and angles equal to those in gaseous alkanes.[69,70] Since it is necessary to assume a conformational structure in order to calculate I_z, the alkyl chains are treated as pure trans-conformers because such configurations are most stable in gaseous species (by 2.5 kJ mol^{-1} per C−C unit over gauche-conformers)[72] and predominate in adsorbed hydrocarbons.[67,68] Although a finite number of other conformers exist,

dx.doi.org/10.1021/ja4093743 | J. Am. Chem. Soc. 2013, 135, 18586−18599

their combined population is less than that of the pure trans-conformers, and consequently we make the simplifying approximation that their contributions to the degrees of freedom of the transition state can be treated separately from I_z and $q_{r,1D}$. The values of I_z as a function of the number of carbon atoms in the alkyl chain are reported in the Supporting Information (Figure S5).

The conformational partition function, q_c, accounts for the probability that the alkyl chains can adopt one of three distinct rotational conformations (trans-, gauche+, and gauche-).[73] These trans and gauche conformations introduce degrees of freedom (and entropy gains) not included in partition functions describing the translational, vibrational, and rotational motions of the activated complex. The value of q_c depends on the number of C−C bonds ($n - 1$, where n is the number of C-atoms) in the n-alkane. The conformational partition function for a linear, α,β-bound hydrocarbon is equal to[73,74]

$$q_c = (n-1)\left(1 + 2\exp\left(\frac{-\Delta H_{gt}}{RT}\right)\right)^{(n-1)} \quad (22)$$

in which ΔH_{gt} is the difference in enthalpy (zero-point vibrational energy) between trans and gauche conformations at each C−C bond (2.5 kJ mol^{-1} per C−C unit).[72]

Partition functions describing translational, vibrational, rotational, and conformational modes of α,β-coordinated species (q_x) are related to entropies by the Sackur−Tetrode equation[59]

$$S_x = k_B \ln(q_x) + k_B T\left[\frac{\partial \ln(q_x)}{\partial T}\right] \quad (23)$$

where x denotes the specific degree of freedom. Figure 8 (a, b) shows that entropies of translation, vibrations, and conformations depend only on the mass and on the total number of C−C and C−H bonds of the transition state (and thus on the chain length of the n-alkane reactant). Rotational entropies, however, differ depending on the location of the α,β C-atoms (the points of attachment to the surface in the one-body transition state) along the chain because this location determines the size of the two pendant alkyl chains and consequently their respective moments of inertia (I_z, Figure S5, Supporting Information). The rotational entropy for the transition state is equal to the sum of the entropies of each independent alkyl chain, which increase monotonically with the length of the alkyl chains (Figure 8). Yet, the greatest and most consequential entropy gains per additional C-atom occur when the number of C-atoms in the alkyl chain increases from 1 to 2 (Figure 8), while the addition of subsequent C-atoms lead to smaller gains in rotational entropy. The amount of rotational entropy gained by increasing the length of an alkyl chain by one carbon atom reflects the natural logarithm of the ratio of I_z values for chains with $n + 1$ and n C-atoms (eqs 20, 21, 23). I_z increases rapidly (eq 21) when the first C-atom is added to the α or β C-atom (i.e., the transition from methylidyne to ethylidyne), but the exponential dependence of I_z on n decreases slightly for $n > 3$ (Figure S5, Supporting Information). For example, $S^{\ddagger}_{r,1D}$ for a single alkyl chain increases by 32 J mol^{-1} K^{-1} as pendant chains grow from 1 to 3 C-atoms (Figure 8), but only by 17 J mol^{-1} K^{-1} as they grow from 3 to 10 C-atoms. Such nonlinear effects lead to entropies that favor nonterminal over terminal C−C bond cleavage in n-alkanes. The translational, vibrational, and conformational entropies (Figure 8 (a, b)) of these transition states are much greater than their rotational entropies

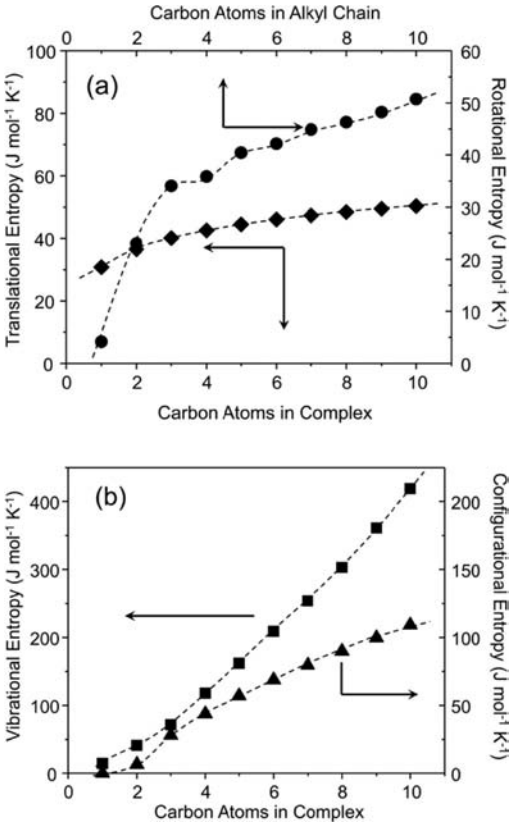

Figure 8. (a) Two-dimensional translational entropy (♦) as a function of the number of carbon atoms and one-dimensional rotational entropy (●) as a function of the number of carbon atoms, i.e., the length, of the alkyl chain assuming an all-trans conformer on an Ir surface. (b) Vibrational entropy (■) as a function of the number of carbon atoms that determine the number of normal modes of the α,β-coordinated surface intermediate and conformational entropy (▲) as a function of the number of carbon atoms the complex on an Ir surface.

(Figure 8 (b)) and account for hydrogenolysis turnover rates that increase markedly with increasing n-alkane length. Yet, rotational entropies, the smallest contributor to total entropy, represent the sole entropic determinant of the position of C−C bond cleavage in a given n-alkane, because such entropies reflect partition functions that are sensitive to the length of the two alkyl chains pendant to the α,β C-atoms bound to the surface.

The total transition state entropy ($S^{\ddagger}$) is given by

$$S^{\ddagger} = S^{\ddagger}_{t,2D} + S^{\ddagger}_{v} + S^{\ddagger}_{r,1D} + S^{\ddagger}_{c} \quad (24)$$

The $S^{\ddagger}$ estimates from statistical mechanics can be compared to $S^{\ddagger}$ values calculated for the cleavage of each type C−C bond within each n-alkane (e.g., the five distinct C−C bonds in n-decane) using eq 15, measured $\Delta S^{\ddagger}$ values, and S_{H2}, S_{H^*}, and S_{RH} calculated from statistical mechanics (Table 2).[59] We note that the analytical model for $S^{\ddagger}$, described in eqs 15−23, does not include any adjustable parameters. Figure 9 shows such a comparison of $S^{\ddagger}$ values for complexes that cleave each distinct C−C bond in the six n-alkanes used in this study on Ir, Rh, and Pt cluster surfaces. Experimental and predicted values of $S^{\ddagger}$ on 0.7 nm Ir clusters agree very well (the slope of the correlation is 1.01 ± 0.03, the intercept is −7 ± 15 J mol^{-1} K^{-1}, and goodness of fit is 0.99). Predictions for $S^{\ddagger}$ match measured $S^{\ddagger}$ values for ethane and n-hexane hydrogenolysis on both 1.3 and 2.7 nm Ir clusters, as well as on small Rh (0.9 nm) and

dx.doi.org/10.1021/ja4093743 | J. Am. Chem. Soc. 2013, 135, 18586−18599

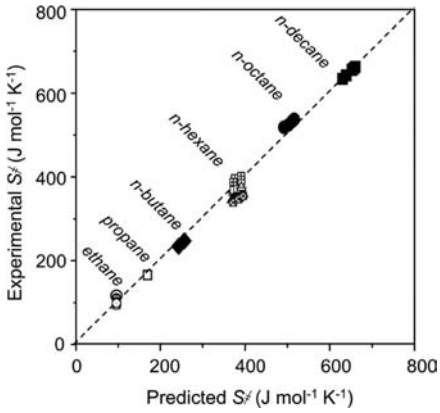

Figure 9. Correlation between predicted transition state entropies, calculated using the described partition functions, and experimental transition state entropies calculated assuming that chemisorbed hydrogen behaves as a two-dimensional ideal gas. Values determined on hydrogen-covered surfaces of 0.7 nm Ir (ethane (○), propane (□), *n*-butane (♦), *n*-hexane (▲), *n*-octane (●), and *n*-decane (■)); 1.3 nm Ir (ethane (⊖), *n*-hexane (dashed △)); 2.7 nm Ir (ethane (⊙), *n*-hexane (⊡)); 0.6 nm Pt (ethane (⊗), *n*-hexane (boxed X)); and 0.9 nm Rh (ethane (⊕), *n*-hexane (⊞)) clusters at 20 kPa alkane. For *n*-alkanes with distinguishable C−C bonds multiple points represent transition state entropies, predicted and measured, for C−C bond rupture at each position.

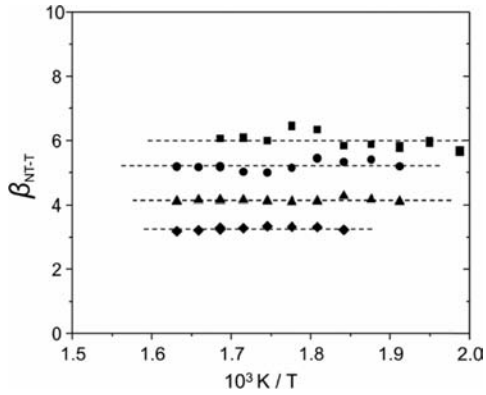

Figure 10. Ratios of the rates of nonterminal to terminal hydrogenolysis, $\beta_{NT\text{-}T}$, for *n*-butane (♦), *n*-hexane (▲), *n*-octane (●), and *n*-decane (■) on hydrogen-covered surfaces of 0.7 nm Ir clusters at 20 kPa alkane. Values of $\beta_{NT\text{-}T}$ are normalized to reflect the occurrence of each type of C−C bond within each *n*-alkane.

Pt (0.6 nm) clusters (Figure 9). These comparisons confirm that the proposed transition state structure (Figure 7), and the identity of the elementary steps and their specific kinetic and thermodynamic relevance (Scheme 1) accurately describes the reactivity and selectivity of surfaces for hydrogenolysis of *n*-alkanes. These factors are apparently independent of the elemental identity or size of the metal clusters. Recent work by Campbell et al. shows that weakly adsorbed gases lose the entropy of one-dimension of free translation with respect to the gas-phase species and ∼1/3 of the entropy associated with the remaining translational, rotational and vibrational degrees of freedom in the gas-phase.[75] Earnest attempts to use this alternate model to describe the entropy of transition states for C−C bond cleavage in these deeply dehydrogenated, and strongly bound, hydrocarbons were unsuccessful in predicting the entropy of these complexes or entropy differences between transition states that cleave C−C bonds at different positions. However, such a model may well describe the entropy of more mobile transition states that mediate other reactions at surfaces,[75] but which are not relevant to catalytic hydrogenolysis. Subsequent publications[46−48] will show that hydrogenolysis of isoalkanes and cycloalkanes on metals can also be rigorously described by these kinetic and thermodynamic formalisms, which appear to be fundamental features of metal-catalyzed hydrogenolysis.

3.4. Enthalpic and Entropic Factors and the Location of C−C Bond Cleavage. Activation energies are likely to show the largest differences between nonterminal (^{2}C−^{2}C) and terminal (^{2}C−^{1}C) bonds in C_{4+} *n*-alkanes, because these bonds differ most markedly in their BDE(C−C)[53] and in their steric access to surface atoms.[58] The ratios of nonterminal to terminal hydrogenolysis rates (β_{NT-T}; eq 9) reflect enthalpy and entropy differences between the transition states that mediate the cleavage of bonds at nonterminal and terminal positions:

$$\beta_{NT-T} = \frac{\sigma_T}{\sigma_{NT}} e^{(S_{NT}^{\ddagger} - S_T^{\ddagger})/R} \cdot e^{-(H_{NT}^{\ddagger} - H_T^{\ddagger})/RT} \frac{P_{H_2}^{\lambda_T}}{P_{H_2}^{\lambda_{NT}}} \quad (25)$$

Figure 10 shows that β_{NT-T} values for *n*-butane, *n*-hexane, *n*-octane, and *n*-decane are independent of temperature on 0.7 nm Ir, indicating that $\Delta H^{\ddagger}$ values for ^{2}C−^{2}C and ^{2}C−^{1}C bond cleavage are actually similar (within experimental uncertainty, ± 2 kJ mol^{-1}) for these larger *n*-alkanes. Therefore, entropy differences between the transition states ($\partial S^{\ddagger}$) for terminal and nonterminal cleavage determine the relative rates of location of C−C bond cleavage for a given *n*-alkane. $\Delta H^{\ddagger}$ for ^{2}C−^{1}C bonds in *n*-alkanes decrease with *n*-alkane chain length (Table 2), even though the BDE(C−C) values for these bonds are similar (360 ± 4.2 kJ mol^{-1}).[53] $\Delta H^{\ddagger}$ values for ^{2}C−^{1}C bonds in propane (230 kJ mol^{-1}) are larger than for ^{2}C−^{1}C bonds in n-butane (228 kJ mol^{-1}) and in longer *n*-alkanes (217 kJ mol^{-1}), because dispersion forces that scale with the number of C-atoms in *n*-alkanes[50] have attractive interactions with the catalyst surface.[76] These interactions stabilize both the transition states and the adsorbed reactants, however, because all steps that precede C−C bond rupture are quasi-equilibrated the stability of the reactants does not influence rates or selectivities. As shown above (Figure 10), β_{NT-T} is unaffected by temperature and larger than unity for all *n*-alkanes that contain terminal and nonterminal C−C bonds because transition state entropies are larger for nonterminal than terminal C−C bond cleavage.

The effects of temperature on the ratio of turnover rates for a given C−C bond to those for the terminal C−C bond in a given *n*-alkane (β_x, *x* denotes the bond position, with 1 assigned to the terminal position) can be used to determine differences in $H^{\ddagger}$ and $S^{\ddagger}$ between two C−C bonds:

$$\beta_x = \frac{\sigma_1}{\sigma_x} e^{(S_x^{\ddagger} - S_1^{\ddagger})/R} \cdot e^{-(H_x^{\ddagger} - H_1^{\ddagger})/RT} \frac{P_{H_2}^{\lambda_1}}{P_{H_2}^{\lambda_x}} \quad (26)$$

Figure 11 shows that β_x values for the three distinct C−C bonds in *n*-hexane are insensitive to temperature, consistent with similar $\Delta H^{\ddagger}$ values for all C−C bonds in *n*-hexane on 0.7 nm Ir. The β_3 value is the largest (the central C−C bond in *n*-hexane) (6.0 ± 0.5) and β values decrease as C−C bonds approach the end of the chain (β_2 is 3.5 ± 0.7). The data in Figure 11 show that the cleavage of terminal C−C bonds is unfavorable, because they have the smallest transition state entropy ($S^{\ddagger}$) within each *n*-alkane. The temperature independence of β_x for n-butane, *n*-hexane, n-octane, and n-decane show

dx.doi.org/10.1021/ja4093743 | J. Am. Chem. Soc. 2013, 135, 18586−18599

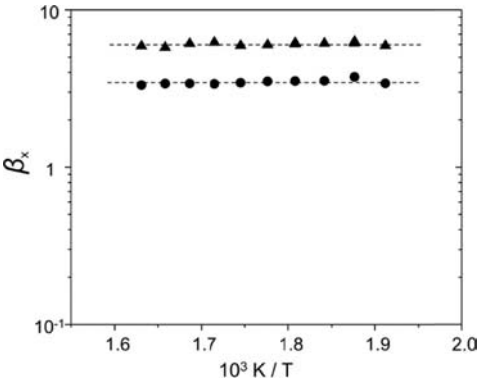

Figure 11. Changes ratios of measured hydrogenolysis rates at indicated positions in *n*-hexane to the rate of terminal C−C bond hydrogenolysis with reciprocal temperature: β_2 (●) and β_3 (▲) on hydrogen-covered surfaces of 0.7 nm Ir clusters at 20 kPa alkane. Subscripts identify the position of the C−C bond from the end of *n*-hexane.

that $\Delta H^{\ddagger}$ values for all C−C bonds within a given alkane are equal on 0.7 nm Ir (within experimental uncertainty, Table 2). These data show that the preference for cleaving nonterminal C−C bonds in all *n*-alkanes merely reflects the differences in entropy among the transition states that mediate C−C bond cleavage at each position.

Figure 12a shows experimental $\partial S^{\ddagger}$ values, which reflect entropy differences between transition states, for a specific nonterminal C−C bond and the terminal C−C bond.

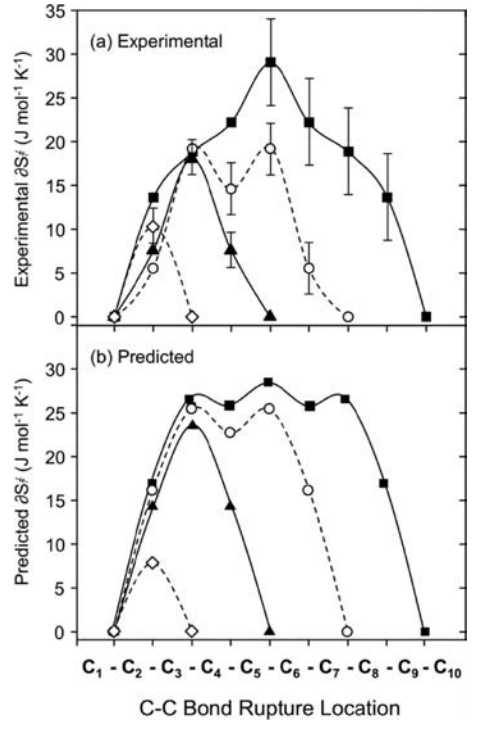

Figure 12. Experimental (a) and predicted (b) differences in transition state entropies, $\partial S^{\ddagger}$, between cleaving C−C bonds at a given positions in the *n*-alkane and the terminal C−C bond, shown for *n*-butane (◊), *n*-hexane (▲), *n*-octane (○), and *n*-decane (■). Experimental values were measured on hydrogen-covered surfaces of 0.7 nm Ir clusters at 20 kPa alkane, and uncertainties represent 95% confidence intervals. Subscripts on the abscissa denote the position of the carbon atoms for each C−C bond (e.g., C_1−C_2 is the terminal bond).

The entropic preference for rupture of a C−C bond increases with its distance from the end of the *n*-alkane chain. Experimental (Figure 12a) and predicted (Figure 12b) $\partial S^{\ddagger}$ values for *n*-octane show oscillations that arise solely from differences in $S_{r,1D}{}^{\ddagger}$. Similar oscillatory behavior is predicted for *n*-decane, but it is made indistinct by uncertainty in the experimental $\partial S^{\ddagger}$ values. These uncertainties are due to impurities found only in the n-decane reactant that continuously deactivated the catalyst, which caused selectivities (at constant conversion) to change over time perhaps as a result of S-accumulation on Ir clusters. The oscillations in $\partial S^{\ddagger}$ (Figure 12b, *n*-octane and *n*-decane) result from non- linear increases in $S_{r,1D}{}^{\ddagger}$ with increasing chain length of each alkyl chain, as given by eqs 20, 21, and 23. These results and their mechanistic interpretation specifically demonstrate that statistical mechanics can be used to predict rates and selectivities of hydrogenolysis reactions on metal clusters.

The elementary steps (Scheme 1), rate expression for H*-covered surfaces (eq 12), and thermochemical cycle (Scheme 2) presented here are *not* specific to *n*-alkanes or to the particular Ir, Rh and Pt cluster catalysts used in this study. Our analysis can be broadly applied to hydrogenolysis reactions of different hydrocarbons (C−C bond rupture), as well as to hydrogen-assisted heteroatom removal (C−S, C−N, and C−O bond rupture), because the foundation of the approach is fundamental and not limited to C−C bond chemistry. In general, C−C bond cleavage occurs via similar pools of quasi- equilibrated dehydrogenated organic reactants on many late transition metals (Ir, Ru, Rh, and Pt); and hydrogenolysis reactions of isoalkanes and cycloalkanes can be rigorously treated using similar formalisms, as we demonstrate in later publications.[46−48]

4. CONCLUSIONS

Hydrogenolysis of C−C bonds in *n*-alkanes occurs on Ir, Rh, and Pt clusters (0.6−2.7 nm in diameter) is accurately described over wide-ranges of temperatures, pressures, and coverages by a rate expression, which is derived from a series of plausible elementary steps. *n*-Alkane hydrogenolysis rates and C−C bond cleavage selectivities are consistent with kinetically relevant C−C bond rupture that occurs in transition states equilibrated with gaseous alkane reactants, H_2(g), and hydrocarbon- or H*-covered surfaces of metal clusters. By utilizing this chemical equilibrium and saturating the surfaces of metal clusters H*, hydrogenolysis turnover rates can be chemically interpreted using a thermochemical cycle and the tenets of transition state theory to determine the composition and stability of transition states that cleave C−C bonds. $\Delta H^{\ddagger}$ for C−C bond cleavage range are prohibitively large, between 257 and 217 kJ mol^{-1} on H*-covered Ir surfaces and correlate with the average BDE(C−C) of the reactant alkanes. These high $\Delta H^{\ddagger}$ require large $\Delta S^{\ddagger}$ that are achieved by the formation of gaseous H_2, which is produced by displacing two H* from the metal surface and by dehydrogenating the reactant. Rate constants for hydrogenolysis increase strikingly with the length of *n*-alkanes, by 10^8 between ethane and n-decane, as a result of $\Delta S^{\ddagger}$ increasing between ethane and n-decane by 95 J mol^{-1} K^{-1}. Entropic differences also produce distinct selectivity patterns that favor nonterminal C−C bond cleavage within C_{4+} *n*-alkanes. A model based on the principles of statistical mechanics and partitions functions that describe the translational, vibrational, rotational, and configurational freedom of a plausible transition state structure shows that these differences in rates and selectivities result from differences

dx.doi.org/10.1021/ja4093743 | J. Am. Chem. Soc. 2013, 135, 18586−18599

between $S^{\ddagger}$ for C−C bond cleavage. Calculations show that long chain *n*-alkanes retain a much larger fraction of their entropy upon adsorption, in the form of intramolecular vibrations and configurations, which causes hydrogenolysis turnover rates to increase markedly with the length of the *n*-alkane. The position of C−C bond cleavage within *n*-alkanes depends on differences in $S^{\ddagger}$ at intramolecular positions that solely reflect changes in the rotational entropy of pendant alkyl chains of the α,β-bound complex. The model to describe $S^{\ddagger}$ is general and consistent with kinetic measurements of hydrogenolysis on metal clusters of different sizes and elemental identities and with isoalkanes and cycloalkanes. As shown here, quantitative chemical descriptions of heterogeneous catalytic reactions can be developed in order to understand the molecular driving forces that determine rates and selectivities for chemical conversions.

■ ASSOCIATED CONTENT

Supporting Information

Full derivation for the turnover rate expression, activation enthalpies, and entropies for ethane and *n*-hexane on Ir, Rh, and Pt clusters, TEM images and cluster size distributions for the Ir, Rh, and Pt cluster catalysts, and the calculated moments of inertia for the one-dimensional rigid rotation of alkyl chains. This information is available free of charge via the Internet at http://pubs.acs.org.

■ AUTHOR INFORMATION

Corresponding Author

iglesia@berkeley.edu

Notes

The authors declare no competing financial interest.

■ ACKNOWLEDGMENTS

We acknowledge Dr. Chris Kliewer (ExxonMobil) for the TEM images, Dr. Stuart L. Soled (ExxonMobil) for helpful guidance in catalyst synthesis and characterization, and Mr. Omar Kunbargi (UC−Berkeley) for assistance with the acquisition of some of the rate data. Dr. Elif Gurbuz (UC−Berkeley) is gratefully acknowledged for the careful review of this manuscript. Technical discussions with Drs. Sebastian Kunz, Monica Garcia, Brett Loveless, and Robert Carr (UC−Berkeley) are also acknowledged with thanks. Dr. George D. Meitzner is acknowledged with thanks for his technical edits of this manuscript. We are grateful to ExxonMobil Research and Engineering Company for the financial support of the research described in this manuscript.

■ REFERENCES

(1) Lee, J. S.; Locatelli, S.; Oyama, S. T.; Boudart, M. *J. Catal.* **1990**, *125*, 157.
(2) Bond, G. C.; Yahya, R.; Coq, B. *J. Chem. Soc., Faraday Trans.* **1990**, *86*, 2297.
(3) Bond, G. C. *Metal-Catalysed Reactions of Hydrocarbons*; Springer: New York, 2005.
(4) Barron, Y.; Maire, G.; Muller, J. M.; Gault, F. G. *J. Catal.* **1966**, *5*, 428.
(5) Maire, G.; Plouidy, G.; Prudhomme, J. C.; Gault, F. G. *J. Catal.* **1965**, *4*, 556.
(6) Sinfelt, J. H. *J. Phys. Chem.* **1964**, *68*, 344.
(7) Goddard, S. A.; Amiridis, M. D.; Rekoske, J. E.; Cardona-Martinez, N.; Dumesic, J. A. *J. Catal.* **1989**, *117*, 155.
(8) Gault, F. G. *C. R. Hebd. Seances Acad. Sci.* **1957**, *245*, 1620.
(9) Bond, G. C.; Cunningham, R. H. *J. Catal.* **1997**, *166*, 172.
(10) Cimino, A.; Boudart, M.; Taylor, H. *J. Phys. Chem.* **1954**, *58*, 796.
(11) Kemball, C.; Taylor, H. S. *J. Am. Chem. Soc.* **1948**, *70*, 345.
(12) Morikawa, K.; Benedict, W. S.; Taylor, H. S. *J. Am. Chem. Soc.* **1936**, *58*, 1795.
(13) Dartigues, J. M.; Chambellan, A.; Gault, F. G. *J. Am. Chem. Soc.* **1976**, *98*, 856.
(14) Weisang, F.; Gault, F. G. *J. Chem. Soc., Chem. Commun.* **1979**, 519.
(15) Gault, F. G. *Adv. Catal.* **1981**, *30*, 1.
(16) Sinfelt, J. H. *J. Catal.* **1972**, *27*, 468.
(17) Sinfelt, J. H.; Taylor, W. F.; Yates, D. J. C. *J. Phys. Chem.* **1965**, *69*, 95.
(18) Sinfelt, J. H.; Yates, D. J. C. *J. Catal.* **1968**, *10*, 362.
(19) Sinfelt, J. H.; Yates, D. J. C.; Carter, J. L. *J. Catal.* **1972**, *24*, 283.
(20) Yates, D. J. C.; Sinfelt, J. H. *J. Catal.* **1969**, *14*, 182.
(21) Engstrom, J. R.; Goodman, D. W.; Weinberg, W. H. *J. Am. Chem. Soc.* **1988**, *110*, 8305.
(22) Goodman, D. W. *Surf. Sci.* **1982**, *123*, L679.
(23) Anderson, S. L.; Szanyi, J.; Paffett, M. T.; Datye, A. K. *J. Catal.* **1996**, *159*, 23.
(24) Kalakkad, D.; Anderson, S. L.; Logan, A. D.; Pena, J.; Braunschweig, E. J.; Peden, C. H. F.; Datye, A. K. *J. Phys. Chem.* **1993**, *97*, 1437.
(25) Zaera, F.; Somorjai, G. A. *J. Phys. Chem.* **1985**, *89*, 3211.
(26) Bond, G. C.; Slaa, J. C. *J. Mol. Catal.* **1994**, *89*, 221.
(27) Kirlin, P. S.; Gates, B. C. *Nature* **1987**, *325*, 38.
(28) Anderson, J. R.; D.D. Eley, H. P.; Paul, B. W. *Adv. Catal.* **1973**, *23*, 1.
(29) Anderson, J. R.; Avery, N. R. *J. Catal.* **1966**, *5*, 446.
(30) Foger, K.; Anderson, J. R. *J. Catal.* **1979**, *59*, 325.
(31) Walter, C. G.; Coq, B.; Figueras, F.; Boulet, M. *Appl. Catal., A* **1995**, *133*, 95.
(32) Do, P. T.; Alvarez, W. E.; Resasco, D. E. *J. Catal.* **2006**, *238*, 477.
(33) Santikunaporn, M.; Alvarez, W. E.; Resasco, D. E. *Appl. Catal., A* **2007**, *325*, 175.
(34) McVicker, G. B.; Daage, M.; Touvelle, M. S.; Hudson, C. W.; Klein, D. P.; Baird, W. C.; Cook, B. R.; Chen, J. G.; Hantzer, S.; Vaughan, D. E. W.; Ellis, E. S.; Feeley, O. C. *J. Catal.* **2002**, *210*, 137.
(35) Chheda, J. N.; Huber, G. W.; Dumesic, J. A. *Angew. Chem., Int. Ed.* **2007**, *46*, 7164.
(36) Corma, A.; Iborra, S.; Velty, A. *Chem. Rev.* **2007**, *107*, 2411.
(37) Huber, G. W.; Iborra, S.; Corma, A. *Chem. Rev.* **2006**, *106*, 4044.
(38) Stanislaus, A.; Cooper, B. H. *Catal. Rev. Sci. Eng.* **1994**, *36*, 75.
(39) Soled, S. L.; Malek, A.; Miseo, S.; Baumgartner, J.; Kliewer, C.; Afeworki, M.; Stevens, P. A. *Stud. Surf. Sci. Catal.* **2006**, *162*, 103.
(40) Miller, J. T.; Schreier, M.; Kropf, A. J.; Regalbuto, J. R. *J. Catal.* **2004**, *225*, 203.
(41) McVicker, G. B.; Baker, R. T. K.; Garten, R. L.; Kugler, E. L. *J. Catal.* **1980**, *65*, 207.
(42) Choi, M.; Wu, Z. J.; Iglesia, E. *J. Am. Chem. Soc.* **2010**, *132*, 9129.
(43) Boudart, M.; Djega-Mariadassou, G. *The Kinetics of Heterogeneous Catalytic Reactions*; Princeton University Press: Princeton, 1984.
(44) Schneider, M.; Duff, D. G.; Mallat, T.; Wildberger, M.; Baiker, A. *J. Catal.* **1994**, *147*, 500.
(45) Sinfelt, J. H.; Yates, D. J. C. *J. Catal.* **1967**, *8*, 82.
(46) Flaherty, D. W.; Hibbitts, D.; Gürbüz, E. I.; Iglesia, E. Manuscript in review.
(47) Flaherty, D. W.; Uzun, A.; Soled, S. L.; Iglesia, E. To be submitted.
(48) Flaherty, D. W.; Hibbitts, D.; Gürbüz, E. I.; Iglesia, E. To be submitted.
(49) Yaws, C. L. *Yaws' Handbook of Thermodynamic and Physical Properties of Chemical Compounds*; Knovel: New York, 2003.
(50) Anslyn, E. V.; Dougherty, D. A. *Modern Physical Organic Chemistry*; University Science Books: Sausalito, CA, 2006.
(51) Chen, Z.-X.; Aleksandrov, H. A.; Basaran, D.; Rosch, N. *J. Phys. Chem. C* **2010**, *114*, 17683.

(52) Kua, J.; Faglioni, F.; Goddard, W. A. *J. Am. Chem. Soc.* **2000**, *122*, 2309.
(53) McMillen, D. F.; Golden, D. M. *Annu. Rev. Phys. Chem.* **1982**, *33*, 493.
(54) Zhao, Z.-J.; Moskaleva, L. V.; Rosch, N. *J. Catal.* **2012**, *285*, 124.
(55) Garcia, A. R.; Barros, R. B.; Ilharco, L. M. *J. Phys. Org. Chem.* **2008**, *21*, 703.
(56) Cortright, R. D.; Watwe, R. M.; Dumesic, J. A. *J. Mol. Catal. A: Chem.* **2000**, *163*, 91.
(57) Cortright, R. D.; Watwe, R. M.; Spiewak, B. E.; Dumesic, J. A. *Catal. Today* **1999**, *53*, 395.
(58) Delbecq, F.; Sautet, P. *Catal. Lett.* **1994**, 89.
(59) McQuarrie, D. A. *Statistical Mechanics*; University Science Books: Sausalito, CA, 2000.
(60) Hagedorn, C. J.; Weiss, M. J.; Weinberg, W. H. *Phys. Rev. B: Condens. Matter* **1999**, *60*, R14 016.
(61) Clark, A. *The Theory of Adsorption and Catalysis*; Academic Press: New York, USA, 1970.
(62) http://cccbdb.nist.gov/.
(63) Alberty, R. A. *Ind. Eng. Chem. Fund.* **1983**, *22*, 318.
(64) Gross, H.; Campbell, C. T.; King, D. A. *Surf. Sci.* **2004**, *572*, 179.
(65) Lytken, O.; Lew, W.; Campbell, C. T. *Chem. Soc. Rev.* **2008**, *37*, 2172.
(66) Hammond, G. S. *J. Am. Chem. Soc.* **1955**, *77*, 334.
(67) Ilharco, L. M.; Garcia, A. R.; Lopes da Silva, J. *Surf. Sci.* **1997**, *371*, 289.
(68) Yang, M.; Somorjai, G. A. *J. Am. Chem. Soc.* **2004**, *126*, 7698.
(69) *CRC Handbook of Chemistry and Physics*; CRC: Boca Raton, 2011; Vol. 92.
(70) Tait, S. L.; Dohnalek, Z.; Campbell, C. T.; Kay, B. D. *J. Chem. Phys.* **2005**, *122*, 164708.
(71) Krekelberg, W. P.; Greeley, J.; Mavrikakis, M. *J. Phys. Chem. B* **2004**, *108*, 987.
(72) Smith, G. D.; Jaffe, R. L. *J. Phys. Chem.* **1996**, *100*, 18718.
(73) Gellman, A. J.; Paserba, K. R. *J. Phys. Chem. B* **2002**, *106*, 13231.
(74) Paserba, K. R.; Gellman, A. J. *J. Chem. Phys.* **2001**, *115*, 6737.
(75) Campbell, C. T.; Sellers, J. R. V. *J. Am. Chem. Soc.* **2012**, *134*, 18109.
(76) Tait, S. L.; Dohnalek, Z.; Campbell, C. T.; Kay, B. D. *J. Chem. Phys.* **2006**, *125*, 234308.